Cellular/Molecular

The Activation Mechanism of α1 Homomeric Glycine Receptors

Marco Beato, Paul J. Groot-Kormelink, David Colquhoun, and Lucia G. Sivilotti
Department of Pharmacology, University College London, WC1E 6BT, United Kingdom

The glycine receptor mediates fast synaptic inhibition in the spinal cord and brainstem. Its activation mechanism is not known, despite the physiological importance of this receptor and the fact that it can serve as a prototype for other homopentameric channels. We analyzed single-channel recordings from rat recombinant α1 glycine receptors by fitting different mechanisms simultaneously to sets of sequences of openings at four glycine concentrations (10–1000 μM). The adequacy of the mechanism and the rate constants thus fitted was judged by examining how well these described the observed dwell-time distributions, open–shut correlation, and single-channel P_{open} dose–response curve. We found that gating efficacy increased as more glycine molecules bind to the channel, but maximum efficacy was reached when only three (of five) potential binding sites are occupied. Successive binding steps are not identical, implying that binding sites can interact while the channel is shut. These interactions can be interpreted in the light of the topology of the binding sites within a homopentamer.

Key words: **binding; channel; dose-response; gating; glycine; kinetics; patch clamp**

Introduction

Glycine is an important fast inhibitory neurotransmitter in the more caudal portions of the CNS, such as the spinal cord (Legendre, 2001). Glycine receptors belong to the nicotinic superfamily and have a pentameric structure, in which the central ion channel is surrounded by five subunits, each with four transmembrane domains. Five different subunit genes have been cloned so far: α1–α4 and β. Of these, only α subunits can form functional recombinant receptors on their own. These homomeric receptors are thought to be the predominant form in young animals. They are mostly replaced by $\alpha\beta$ heteromers in the adult (Legendre, 2001), although there is evidence for the presence of homomeric glycine receptors in the adult [on brainstem presynaptic terminals (Turecek and Trussell, 2002)].

In contrast with muscle nicotinic receptors, a full kinetic scheme that can account for all of the features observed in glycine single-channel recordings is still lacking. Such a scheme is needed, first of all, for the interpretation of the characteristics of glycinergic synaptic currents, such as the factors that control their time course, degree of postsynaptic receptor saturation, or effects of antagonists on synaptic transmission. Without knowledge of a mechanism, it is also impossible to understand the functional effects of mutations in glycine receptor subunits (for human startle disease mutations, see Rajendra and Schofield, 1995), the nature of the binding site for glycine and other agonists, the process of channel opening, and the link between them (Edmonds et al., 1995; Colquhoun, 1998).

Extending previous work on the concentration dependence of native receptor activation by Twyman and Macdonald (1991), Beato et al. (2002) used low-concentration single-channel recordings to arrive at a preliminary postulated reaction mechanism for the homomeric α1 receptor. However, the most precise results are found by fitting simultaneous recordings made at both low and high concentrations of agonist (Colquhoun et al., 2003a; Hatton et al., 2003). Direct mechanism fitting by maximum likelihood with missed event correction (Hawkes et al., 1992; Colquhoun et al., 1996, 2003a; Qin et al., 1996) to sequences of open and shut times allows us to extract in one operation all of the information contained in the records (including correlations). This method bypasses the need to fit arbitrary mixtures of exponentials to various observed distributions and gives direct estimates of the physical rate constants in any specified mechanism. In this paper, we used simultaneous fitting of recordings at a wide range of concentrations to compare several possible mechanisms for the homomeric α1 receptor and to identify features in the mechanisms that are necessary to describe the data.

Materials and Methods

Homomeric glycine receptors were expressed in human embryonic kidney 293 cells according to the protocol described by Groot-Kormelink et al. (2002). Briefly, cells were transfected by calcium phosphate-DNA coprecipitation with cDNA coding for the rat α1 glycine receptor subunit (GenBank accession number AJ310834) and for the marker protein enhanced green fluorescent protein-c1 (Clontech, Cambridge, UK). The amount of α1 subunit cDNA was chosen to get the optimal level of expression for single-channel recordings (Groot-Kormelink et al., 2002).

All recordings were performed in the cell-attached configuration using glycine as an agonist in the pipette, which was filled with extracellular solution. This was prepared in HPLC-grade water (to minimize the

Received Sept. 30, 2003; revised Nov. 4, 2003; accepted Nov. 4, 2003.

This work was supported by the Medical Research Council (MRC) and Wellcome Trust Project Grant 064652. M.B. is a Computational Biology MRC Training Fellow.

Correspondence should be addressed to Dr. Marco Beato, University College London, Department of Pharmacology, Gower Street, WC1E 6BT, London, UK. E-mail: m.beato@ucl.ac.uk.

DOI:10.1523/JNEUROSCI.4420-03.2004

 0270-6474/04/240895-12$15.00/0

amount of contaminating glycine) and contained the following (in mM): 102.7 NaCl, 20 Na gluconate, 4.7 KCl, 2 $CaCl_2$, 1.2 $MgCl_2$, 10 HEPES, 14 glucose, 15 sucrose, and 20 TEACl, adjusted to pH 7.4 with NaOH. Electrode resistance was in the range of 10 to 15 MΩ. The computer programs used in the analysis (SCAN, EKDIST, HJCFIT, CVFIT, and SCALCS) are available at http://www.ucl.ac.uk/Pharmacology/dc.html.

The Hill equation was fitted to P_{open}-concentration data using CVFIT, and P_{open}-concentration curves were calculated in SCALCS, for each reaction scheme using the fitted rate constants. The program also gives a value for the Hill slope at EC_{50}, this slope being defined as:

$$\left.\frac{d\ ln\left(\frac{P_{open}}{P_{max} - P_{open}}\right)}{d\ ln(G)}\right|_{G\,=\,EC50}, \quad (1)$$

where G is the glycine concentration.

Recordings were obtained with an Axopatch 200B amplifier (Axon Instruments, Foster City, CA), prefiltered at 10 kHz (with the amplifier 4-pole Bessel filter), stored on a DAT tape, and then filtered at 3 kHz with an 8-pole Bessel filter and digitized using Axon Instruments software at 30 kHz sampling rate for off-line analysis. Open times, shut times, and amplitudes were idealized with SCAN, and dwell time distributions were fitted with mixtures of exponential densities using the EKDIST program after imposing a resolution of 30 μs. For each experiment, 15,000–25,000 transitions were fitted.

Clusters of activations separated by long (between approximately 1 and 100 s) sojourns in desensitized states (Colquhoun and Ogden, 1988) were detected at all concentrations of glycine greater than 10 μM. At 50 μM, 100 μM, and 1000 μM, it was possible to be almost sure that all openings within a cluster came from the same channel, so they could be used for the calculation of the probability of being open, P_{open} (i.e., the fraction of time for which the channel is open, estimated as the ratio between the total open time per cluster and the cluster length) (see Results).

The HJCFIT program was used to obtain maximum likelihood estimates of the rate constants for each of the mechanisms tested (Colquhoun et al., 1996, 2003a; Hatton et al., 2003). To calculate lengths of observed openings and shuttings, correction for missed events is essential, and the program uses the exact missed event correction of Hawkes, Jalali, and Colquhoun (Hawkes et al., 1990,1992), with "HJC" being an acronym from the authors' names.

Most of the mechanisms that were tried are shown in Figures 3 and 8, with the symbol assigned to each of the rate constants. In all mechanisms tested, it was assumed that dissociation from open states is negligible. This is not likely to be exactly true, but dissociation from open states is likely to be so slow that little error will result from neglecting it (Grosman and Auerbach, 2000; Beato et al., 2002).

A total of 16 cell-attached experiments at 10, 50, 100, and 1000 μM glycine was fitted simultaneously in six sets of four, each set containing one experiment for each of the above concentrations as described by Colquhoun et al. (2003a) and Hatton et al. (2003) (three of the patches at 10 and 50 μM and two of the patches at 1000 μM were used twice so that eight experiments appeared twice in distinct sets). Briefly, the program calculates the likelihood of the entire sequence of open and shut times (in the order in which they occur) from the postulated mechanism and a set of initial guesses for the rate constants. The rate constants are then adjusted iteratively to maximize the likelihood of the entire sequence. Openings were divided into groups by means of a critical shut time, t_{crit}, such that all openings within a group are likely to come from the same channel. At 10 μM glycine, these groups will correspond approximately to individual activations of the channel. The likelihood for each group at 10 μM was calculated using initial and final vectors, which are denoted, as an acronym, as CHS vectors because they were defined by Colquhoun, Hawkes, and Srodzinski (Colquhoun et al., 1996, Eqs. 5.8, 5.11). If there is more than one channel in the patch, adjacent groups of openings may come from different channels; thus the true (one channel) shut time is not known, but the use of CHS vectors exploits information from the knowledge that it must be more than t_{crit}. At 100 μM and 1000 μM glycine, desensitization is prominent, and thus CHS vectors cannot be used, because desensitized states are not included in the mechanisms (see Figs. 3, 8). In this case, steady-state vectors were used, which is a procedure that can be justified by the results of simulations (Colquhoun et al., 2003a). At 50 μM, the correct procedure is less obvious; however, similar results were obtained with CHS vectors and steady-state vectors (the former were used for the results given here).

At the highest concentration, it was found necessary to exclude arbitrarily a few shut times from the analysis. The t_{crit} for the experiments at 1000 μM was set to a short value, 0.6–0.8 ms, to exclude, as far as possible, the last small component in the shut times distribution (see Fig. 2*d*, Table 2). This had very little effect on the fits, because the excluded shut times are very rare (usually not more than 20–30 of 9000–10,000 shut times). Furthermore, none of the fits of the schemes in Figure 3 could generate an apparent (HJC) shut-time distribution that described this very small component. This does not affect our conclusions, because inclusion of this small number of shut times made little difference to the estimates of either the rate constants or the P_{open}. For example, P_{open} at 1000 μM was 0.96 ± 0.01 with the extra shut times and 0.97 ± 0.01 without the extra shut times. These shut times presumably arise from an infrequently visited state that is not included in the mechanism being fitted. They might, for example, be similar to the extra "1 ms shut state" postulated by Salamone et al. (1999) for the mouse muscle-type nicotinic receptor; although, for the human wild-type nicotinic receptor, the existence of such a state is dubious (Colquhoun et al., 2003a; Hatton et al., 2003). Introduction of an extra shut state connected to the fully liganded shut or open states in either Scheme 1 or Scheme 2 gave a slightly better fit of the long (1 ms) shut-state component at 1000 μM without altering the fits at lower concentrations. However, whereas the estimate of the rate constant to exit the extra shut state was well defined (3600 s^{-1} ±11%), the rate of entry into it was poorly determined (2600 s^{-1} ±66%), probably because of its infrequent occurrence.

After estimation of the rate constants, the quality of the fit was assessed by visual inspection of the agreement of the predicted (HJC) distributions with the experimental results using four criteria: open and shut times, correlations, and the P_{open} curve (see Figs. 4–7, 9). The predicted (HJC) distribution for a given mechanism, rate constants, and resolution was superimposed on (not fitted to) the experimental distributions of open and shut times. The adequacy of the prediction of correlations was examined by comparing the calculated and observed mean open periods for events adjacent to shut times in specified ranges (a conditional mean plot). The calculated values are found as described previously (Colquhoun et al., 1996, sections 3 and 4). Finally, the extent to which the fitted rate constants could predict the experimental P_{open} curve was inspected. All of these criteria allowed us to exclude some of the proposed models as described in Results. Data are expressed as mean ± SD of the mean. For estimated rate constants, we report the average of different sets of fits and the coefficient of variation of the mean.

Results

General features of single channels

Steady-state experiments at 10–1000 μM glycine, illustrated in Figure 1, were fitted initially without reference to mechanisms (Fig. 2) (EKDIST program). As in outside-out patch recordings (Beato et al., 2002), in all experiments, only one single-channel amplitude was detected, on average 4.7 ± 0.1 pA (Gaussian fit; $n = 26$). This is in contrast to the several conductance levels commonly reported for homomeric glycine receptors (Bormann et al., 1993; Lewis et al., 1998; but see Lewis et al., 2003). We do not know the reason for these discrepant reports. Possible contributions may come from differences in the methods of analysis, species (human vs rat clones), receptor heterogeneity, and vagaries of expression systems.

At 10 μM glycine, individual activations of the channels occur as bursts of openings separated by longer shut times that reflect primarily long sojourn(s) in the unliganded state, although some desensitization may well be present (Fig. 1*a*). Increasing the concentration of glycine causes the receptors to enter into long-lived

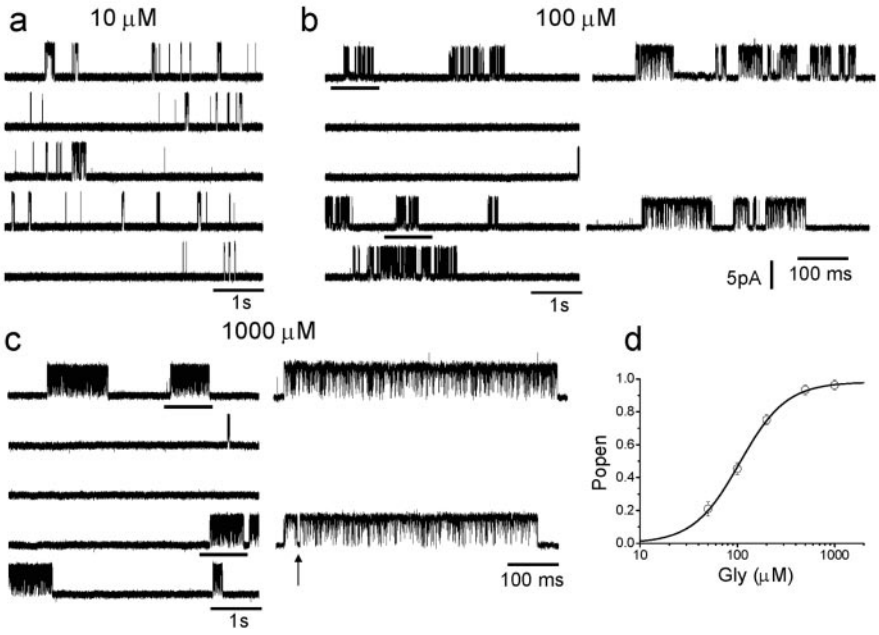

Figure 1. Clustering of α1 glycine receptor openings at increasing agonist concentrations. *a–c*, Continuous sweeps recorded in the cell-attached patch configuration showing channel openings elicited by 10, 100, and 1000 μM glycine in the recording electrode. The sweeps shown to the right of *b* and *c* are expanded displays of two clusters in the continuous record (indicated by a bar under the recording). The arrow in the expanded time scale trace of *c* marks an example of a long (~5 ms) shut state within the cluster. Note that bursts of openings are observed at the lower concentration; at the higher agonist concentrations, these bursts group into progressively longer clusters with increasing P_{open}. *d* shows a P_{open} dose–response curve. P_{open} values are obtained for each cluster from the ratio between total open time (obtained from records idealized by time course fitting) and total duration. The points shown are the averages of 34–50 clusters for each glycine concentration. Here, these points are fitted by a Hill equation (solid line).

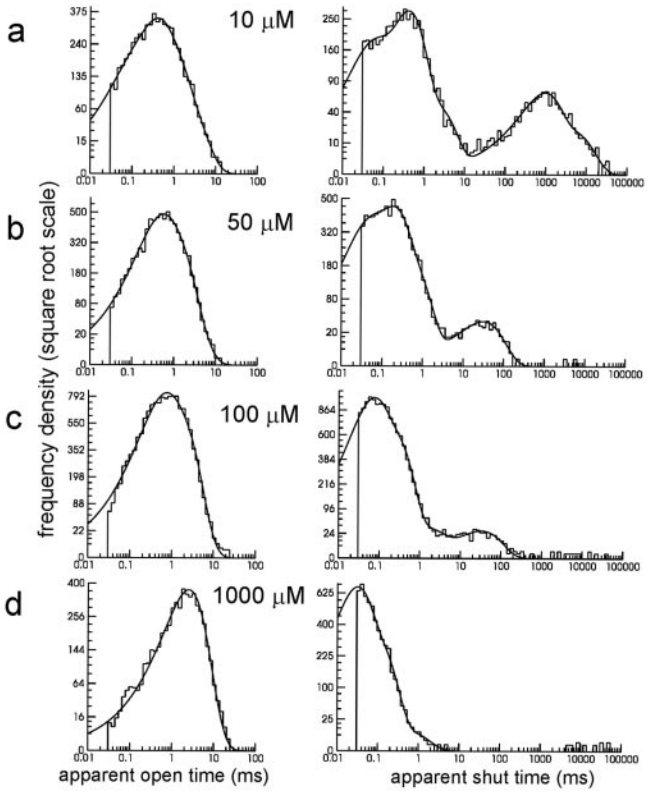

Figure 2. *a–d*, Dwell-time distributions for cell-attached recordings at increasing glycine concentrations. Both open-time and shut-time distributions were fitted with mixtures of exponential components. The results are given in Tables 1 and 2.

desensitized states (Takahashi and Momiyama, 1991). This is clearly seen at both 100 and 1000 μM glycine (Fig. 1,*b* and *c*, respectively). Clusters are separated by long (1–10 s) shut times, and each cluster contains many activations. Clusters at 1000 μM glycine have a high P_{open} (approximately 0.96) and contain only short shuttings (Fig. 1*c*, left, expanded display), whereas clusters at 100 μM glycine ($P_{open} \approx 0.45$) contain longer shut times (5–100 ms) (Fig. 1*b*, right panel). The results of empirical fitting with exponentials (EKDIST) are summarized in Tables 1 and 2, and examples of fitted distributions are shown in Figure 2.

Open-period distributions are fitted with three exponential components (10 μM), two exponential components (50, 100, 200, and 500 μM), or one exponential component (1000 μM). The overall mean open period increases from 0.7 ± 0.1 ms at 10 μM to 2.7 ± 0.2 ms at 1000 μM. This reflects a progressive increase in the area of the slowest component from 22 ± 2 to 100% for increasing concentration of agonist, whereas the time constants for each component are similar at all concentrations (as found by Beato et al., 2002, over a smaller range of concentrations).

Shut-time distributions were fitted with three or four components (Fig. 2, Table 2). For the distributions observed at 10 μM, the first (shortest) three components had time constants that were similar for the different patches and were therefore considered to be within bursts. The average t_{crit} was 8.2 ± 1.6 ms (chosen to have the same proportion of short and long misclassified events as in Colquhoun and Sakmann, 1985). Empirical fits of within-cluster shut-time distributions showed that four components were detectable at 50 and 100 μM glycine and three at higher concentrations. The fastest three time constants (approximately 30 μs, 0.2 ms, and 1.5 ms) were similar at all concentrations tested. Note that such empirical fits are not used for the model fitting (see Materials and Methods and below), and, therefore, it is not important whether all components can be detected.

The P_{open} concentration–response curve

In the experiments shown in Figure 2, the separation into clusters was almost unambiguous (at 50, 100, and 1000 μM), because the inter-cluster intervals are two orders of magnitude longer than the longest of the other shut-time components.

Only a few clusters (3–25) were analyzed for each experiment, because one cluster can contain up to 10,000 transitions. For each individual cluster, the P_{open} was estimated as the ratio between the total open time per cluster and the cluster length. Average P_{open} values are given in Table 3 and plotted as a concentration–response curve in Figure 1*d*. When fitted empirically with the Hill equation, this gave an EC_{50} of 106 ± 8 μM (two-unit likelihood interval, 91–124 μM; this corresponds to a 95% confidence interval; Colquhoun and Sigworth,1995) (weighted least squares fit, errors from observed information matrix; CVFIT program, http://www.ucl.ac.uk/Pharmacology/dc.html), a Hill slope of 1.82 ± 0.24 (two-unit likelihood interval, 1.37–2.36), and a maximum

Table 1. Fits to distributions of open-period durations

Gly (μM) (*n*)	τ_1 (ms) Area (%)	τ_2 (ms) Area (%)	τ_3 (ms) Area (%)	Mean open time (ms)
10	0.13 ± 0.05	0.5 ± 0.1	1.5 ± 0.1	0.7 ± 0.1
(4)	(18 ± 8%)	(60 ± 7%)	(22 ± 2%)	
50	—	0.4 ± 0.1	1.5 ± 0.2	1.0 ± 0.1
(5)		(50 ± 1%)	(50 ± 1%)	
100	—	0.5 ± 0.1	2.1 ± 0.4	1.3 ± 0.2
(6)		(51 ± 6%)	(49 ± 5%)	
200	—	0.4 ± 0.1	2.0 ± 0.1	1.5 ± 0.1
(2)		(24 ± 6%)	(76 ± 7%)	
500	—	0.4 ± 0.1	2.8 ± 1.0	1.7 ± 0.1
(4)		(15 ± 4%)	(85 ± 4%)	
1000	—	—	2.7 ± 0.2	2.7 ± 0.2
(5)			(100%)	

Distribution of open periods was fitted with mixtures of exponential components. The exponential time constant of each component and its relative area (in parentheses) are given as mean ± SD of the mean. Note the increase in the area of the slowest component with increasing concentration of agonist.

P_{open} of 0.98 ± 0.03 (two-unit likelihood interval, 0.92–1.05). The P_{open} concentration–response curve (Sine and Steinbach, 1987; Colquhoun and Ogden, 1988; Sine et al., 1990) represents an "ideal" dose–response curve in that it is corrected for desensitization, contrary to what inevitably occurs for macroscopic dose–response curves, regardless of the speed of the perfusion system. Indeed, it is likely that the impact of desensitization on macroscopic responses explains why such concentration–response curves have lower EC_{50} (within the 30–80 μM range) and higher Hill slopes than those obtained by single-channel recording (Bormann et al., 1993; Rajendra et al., 1994; Beato et al., 2002). Note also that only the P_{open} concentration–response curve can give us an estimate of the maximum P_{open} value, because it is measured on an absolute scale, rather than a relative scale. These three parameters, EC_{50}, Hill slope, and maximum P_{open}, should be predicted accurately by the rate constants that are fitted by HJCFIT, a test that is applied below.

Although ideal in principle, P_{open} curves are themselves subject to errors, and, in view of the surprisingly low Hill slope, these were checked. (1) Is there only one active channel? The lack of double openings within each cluster confirms that only one channel is active within the cluster. In fact, if two channels were simultaneously active, even for the lowest observed average P_{open} (0.2 at 50 μM), the probability of observing even a few openings without any doubles is very low (less than 0.001% for 60 consecutive openings) (Colquhoun and Hawkes, 1990, 1995). It is true that a short cluster might superimpose on a longer one without producing a double opening, but the reproducibility of the P_{open} values makes this unlikely. (2) Are the appropriate shut times included in clusters? The t_{crit} value used to define clusters is inevitably imperfect. The clearest example is seen in the experiments at 100 μM glycine, where a t_{crit} of 400–500 ms includes in the clusters the extra long shut times observed in the tail of the slowest component of the shut-time distribution (Fig. 2) at 100 μM glycine. To address this problem, P_{open} calculations were repeated with a lower t_{crit} (100–150 ms) that excluded these extra long shut times. These events were very few (on average, three to four in each of the six experiments) and reclassifying them increased the number of separated clusters from 46 to 67 but did not change the P_{open} (0.47 ± 0.03, very close to the value measured with the higher t_{crit}, 0.45 ± 0.04). This is probably because clusters at this concentration of glycine are very long (approximately 2 s), and including a few shut times of approximately 200 ms has but little effect on the total P_{open}. When the whole P_{open} curve was refitted using the lower t_{crit}, the estimate of the Hill slope barely changed (from 1.82 to 1.78). (3) Are estimates of P_{open} values affected by missed shut times within a cluster? This problem is potentially most serious at the highest glycine concentration (1 mM). An approximate estimate of the time occupied by the missed shut times (Colquhoun and Sakmann, 1985) showed that missing shut times would at worst increase the P_{open} at 1 mM glycine by 0.4%. Note that the correction assumes that no openings are missed (a reasonable approximation, given that we miss approximately 4% of openings and 51% of shut times at this concentration).

Fitting mechanisms to the data: five binding sites

Some of the mechanisms that were fitted are shown in Figure 3. Experimental records were divided into groups of openings that were thought to come from one channel (see Materials and Methods). For 10 and 50 μM, the t_{crit} was chosen between the third and fourth components of the shut-time distribution. For experiments at 100 μM, the t_{crit} was between 200 and 500 ms to include all shut times within the cluster and to exclude the longer (1–100 s) sojourns in desensitized states that separate clusters. The t_{crit} for the experiments at 1000 μM was set to a much shorter value, 0.6–0.8 ms, to exclude as far as possible the last small component in the shut-time distribution (Fig. 2*d*, Table 2) (see Materials and Methods). An example of a shut time in this component is indicated by the arrow in Figure 1*c* (see Materials and Methods).

In choosing putative mechanisms, we started from the simplest plausible physical assumption. Homomeric glycine receptors have five identical subunits and thus a maximum number of five symmetrical binding sites. Therefore, our first guess includes five binding sites that are initially identical. In the first instance, we also assumed that the binding sites did not interact, so the binding and unbinding rate constants for each (shut) site are not affected by occupancy of the others. This assumption is specified by applying the following constraints during the fitting of Scheme 1 (Fig. 3).

$$k_{+1} = 5k_{+5}, \quad k_{+2} = 4k_{+5}, \quad k_{+3} = 3k_{+5}, \quad k_{+4} = 2k_{+5}$$
$$k_{-5} = 5k_{-1}, \quad k_{-4} = 4k_{-1}, \quad k_{-3} = 3k_{-1}, \quad k_{-2} = 2k_{-1} \quad . \qquad (2)$$

Thus, each agonist binding site is assumed to have the same equilibrium dissociation constant, *K* (Fig. 4*c*), once corrected with the appropriate statistical factors that allow for the number of available sites. To maintain generality, we postulated the existence of one open state for each ligation state of the receptor, and the gating constants for each open state were fitted as free parameters. The resulting fit is shown in Fig. 4.

The histograms in Figure 4 show the open and shut time distributions for the same experiments in Figure 2, and the HJC distributions calculated from the fitted rates (Table 4) are shown (continuous line) superimposed on the observations. The dashed line in each histogram represents the prediction of the distribution that would be observed at ideal resolution (i.e., if no brief events were missed). The difference between this and the continuous line gives a measure of how much the observed distributions are distorted as a result of omission of short open and shut times.

The distributions shown are not simple mixtures of exponentials fitted to the experimental distributions of apparent open or shut periods, as in Figure 2, but are the actual HJC density functions calculated (with exact allowance for missed events) from the rate constants estimated by HJCFIT for this particular mechanism, resolution, and set of observations. The lines will fit the data histogram only if the mechanism used and the estimated rate constants represent an adequate description of the observations.

Table 2. Fits to distributions of shut time durations

Gly (μM) (n)	τ_1 (ms) Area (%)	τ_2 (ms) Area (%)	τ_3 (ms) Area (%)	τ_4 (ms) Area (%)	
10	0.04 ± 0.01	0.3 ± 0.1	1.7 ± 0.3	—	Within bursts
(4)	(33 ± 5%)	(60 ± 2%)	(8 ± 2%)		
50	0.03 ± 0.03	0.21 ± 0.02	0.9 ± 0.2	43 ± 10	Within clusters
(5)	(37 ± 6%)	(46 ± 1%)	(13 ± 5%)	(4 ± 1%)	
100	0.04 ± 0.01	0.21 ± 0.01	1.1 ± 0.2	37 ± 5	Within clusters
(6)	(51 ± 2%)	(42 ± 6%)	(3 ± 1%)	(3 ± 1%)	
200	0.04 ± 0.01	0.20 ± 0.10	1.8 ± 0.1	—	Within clusters
(2)	(52 ± 2%)	(44 ± 6%)	(3 ± 1%)		
500	0.03 ± 0.01	0.16 ± 0.02	1.1 ± 0.2	—	Within clusters
(4)	(64 ± 6%)	(32 ± 6%)	(4 ± 1%)		
1000	0.03 ± 0.01	0.10 ± 0.01	0.50 ± 0.03	—	Within clusters
(5)	(65 ± 2%)	(34 ± 2%)	(1 ± 0.1%)		

Shut-times distribution were fitted with three or four exponential components. The values of the time constants are similar at different concentrations. However, in the experiments at 50 and 100 μM, an extra slow component (~40 ms) was detected. This component represented long-lived shut states observed within clusters.

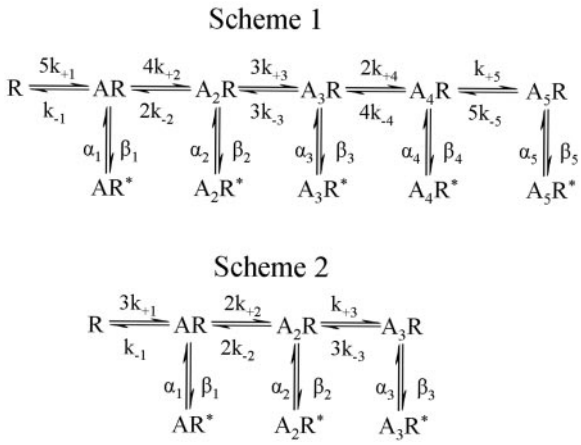

Figure 3. Schematic representation showing the names of the rate constants of some of the mechanisms of receptor activation that were fitted to the single-channel data.

Table 3. Cluster parameters

Gly (μM) (n)	Number of clusters	Cluster length (s)	P_{open}
50 (5)	44	2.2 ± 0.4	0.21 ± 0.04
100 (6)	46	1.9 ± 0.3	0.45 ± 0.04
200 (2)	34	1.6 ± 0.6	0.75 ± 0.03
500 (4)	50	0.7 ± 0.1	0.93 ± 0.03
1000 (5)	45	1.1 ± 0.1	0.96 ± 0.03

Values were obtained from time course fitting of individual clusters. The P_{open} values and the cluster lengths are the average taken from many clusters in different experiments.

In this case, open-period data are well fitted, although there is a little discrepancy for both long and short open periods at 10 μM. However, the fit of the shut times is entirely inadequate at 10 μM, and most of the fast shut time component is not fitted for the three remaining concentrations. The third row of plots shows the predicted and observed correlations between adjacent open and shut times. In each plot, filled diamonds (joined by a continuous line) represent the experimental value for the mean open period adjacent to a shut time in the specified range. For instance, the leftmost symbol in the plot for 10 μM glycine shows that the open times adjacent to the shorter gaps (less than 0.1 ms) were relatively long (on average, approximately 1 ms). The filled circles are the predicted values for the mean open time adjacent to gaps in each of the specified ranges (calculated on the basis of the fitted model and rate constant values). The dashed line is the theoretical continuous relationship between mean open time and adjacent shut time. Correlations were predicted satisfactorily only for the 50 and 100 μM experiments, whereas at the highest and lowest concentrations, the predicted line lies well below the experimental data. Finally, the prediction of the P_{open} dose–response curve was adequate (Fig. 4, bottom). Note that in this and subsequent figures, the curve shown is not a Hill equation but the dose–response relationship predicted by the mechanism; this is not fitted to the P_{open} data points but is calculated from the rate constant value estimated by HJCFIT.

It is possible that the poor agreement of the dwell time distributions with the calculated ones for the fit of Scheme 1 is a result of having imposed unrealistic binding constraints, and that the agonist binding sites do in reality interact while the channel is still shut. In Figure 5, we show a fit of the same data to the same model (Fig. 5*c*) but without any constraints, thus increasing the number of free parameters from 12 to 20.

All dwell-time distributions are now fitted quite well, including the fast shut time components at all concentrations. Furthermore, the predicted correlations were in excellent agreement with the observed data (third row of plots). However, the predicted dose–response curve was too steep (Fig. 5*b*). The predicted EC_{50} and maximum P_{open} (98 μM and 0.98, respectively) were quite good, but the predicted Hill slope (evaluated at the EC_{50}) was much steeper (3.1) than the observed value (1.8). This may be because of the initial positive cooperativity in the binding of the first three molecules (Table 4, rate constants). Similar conclusions were reached for a similar model with four binding sites only; this gave satisfactory fits of dwell-time distributions but a slope at EC_{50} of 2.8 (data not shown). Because five (or four) agonist binding sites predicted a steeper concentration–response curve than we observed (unless the sites were identical and independent, a possibility we have already excluded) (Fig. 4), we next chose to test schemes with a smaller number of binding sites.

Fitting mechanisms to the data: three binding sites

The same combinations of data sets were therefore fitted with mechanisms with two or three binding sites. Two binding sites failed to produce good fits (data not shown), but the mechanism with three binding sites (Fig. 3, Scheme 2) was more promising. Initially, we constrained binding sites to be equal and independent (with the same constraints used for Scheme 1 in the fits of Fig. 4); this gave very poor results (data not shown). We therefore proceeded to perform unconstrained fits for the three-site scheme, allowing interaction between binding sites in the shut conformation ("cooperativity in binding"); these are shown in Figure 6 for the same set of experiments as before.

In this case, all of the dwell-time distributions were fitted ad-

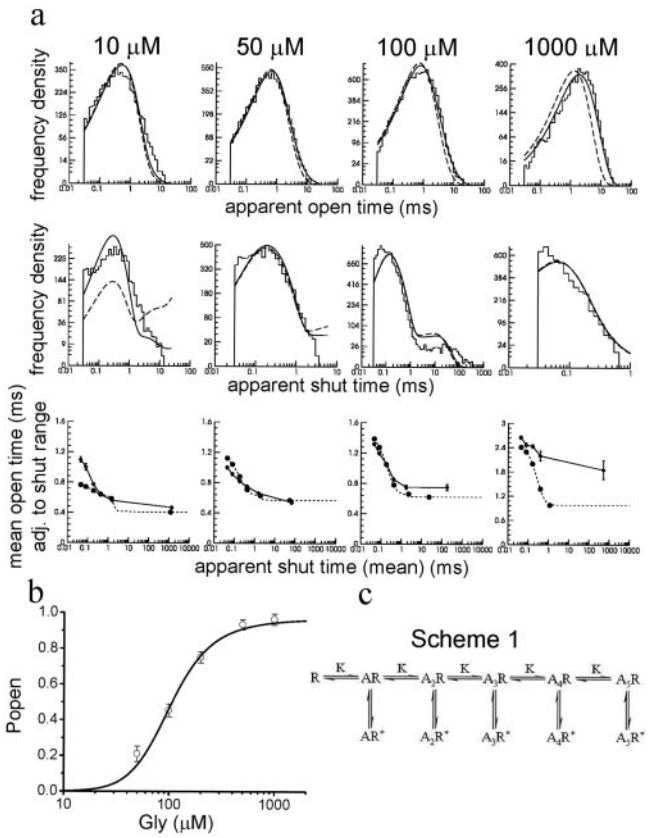

Figure 4. *a*, HJC fitting of Scheme 1 (five binding sites constrained to be the same, *c*) to data from patches at four different glycine concentrations. The distributions (smooth lines superimposed on the open-time and shut-time histograms; top two rows of plots) are calculated from the mechanism rate constants simultaneously fitted to the entire sequence of events at the different agonist concentrations. Solid lines are predicted (HJC) dwell-time distributions corrected for missed events, whereas dashed lines are the distributions expected if no events were missed. The accuracy of the fit in predicting the negative correlation between the length of an opening and the length of the adjacent shut time was tested by the conditional mean plots (third row). Mean open time for openings that are adjacent to shut times in specified ranges (ordinate) are plotted against the mean of the shut times in each range (abscissa). Experimental observations are shown as filled diamonds, ±SD of the mean, and are joined by solid lines. The corresponding values calculated from the fitted rate constants are displayed as filled circles. The dashed line shows the theoretical continuous relationship between open time and adjacent shut time. Note the poor agreement with experimental data, particularly for the shut-time distributions and the correlations at high concentration. *b*, The bottom plot shows the same cluster P_{open} values as Figure 1*d*. The solid line is the equilibrium dose–response relationship predicted by the fitted rate constants and the mechanism (note that this relationship is not a Hill equation and that it is not directly fitted to the data points). *c*, Scheme fitted to the data. The binding sites are constrained to be equal, and this is indicated by the same equilibrium constant (*K*) over the binding steps.

equately, and the dose–response curve calculated from the fitted rate constants was in good agreement with the experimental data. The quality of the correlation plot is also satisfactory, although there is a slight tendency to overestimate the duration of mean open periods for the 50 μM experiment. It is worth noting that some degree of open–shut correlation was still detectable even at 1000 μM. This happens because the occupancy of partially bound open states is not negligible even at this concentration. In particular, the open state with two molecules bound (the lifetime of which is approximately 0.7 ms) has occupancy of 13% at this concentration. The fit shows that efficacy increased with the number of bound molecules, from 0.4 with one bound to 8 with two bound and 43 with three bound (Table 5). Note also that the values of the rate constants were well determined, as seen both from the errors calculated through the Hessian matrix (Colquhoun et al., 2003a; Hatton et al., 2003) and from the coefficient of variation of the mean of each rate constant between different sets of experiments (Table 5).

In contrast, the equilibrium constants for binding do not exhibit such a regular pattern. In fact, the first equilibrium constant (corrected with a statistical factor of 3) was approximately 3200 μM, whereas the second binding equilibrium constant was only 110 μM and the last increased again to 420 μM. In other words, there must be some form of interaction between binding sites in the shut conformation to account for our experimental results, but such cooperative behavior is not regular. Indeed, the first binding is rather low affinity, but the second is much higher, whereas having two bound molecules reduces the affinity of the shut state for the third binding, which is the most important for the operation of the channel in physiological conditions, given that the receptor with three molecules bound has the highest probability of opening. There is no obvious physical interpretation for this mixed cooperativity; however, one possibility is that the model we are using to fit the data is not adequate.

Fitting mechanisms to the data: five binding sites and saturation of gating

Thus, so far, only the mechanism with three unconstrained binding sites has given an adequate prediction of the Hill slope of the P_{open} curve. An obvious question is whether the remaining two binding sites in the receptor pentamer can bind agonist. The fits of a mechanism with five binding sites shown in Figures 4 and 5 did not test the possibility that the binding of a fourth and fifth agonist molecule does occur but does not increase the efficacy of gating beyond that seen with three molecules bound. This can be tested by fitting Scheme 1 while constraining all gating rate constants for receptors with four and five glycine molecules bound to be the same as for those with three bound (*E* in Fig. 7*c*). The constraints were as follows:

$$\alpha_5 = \alpha_4 = \alpha_3, \text{ and } \beta_5 = \beta_4 = \beta_3 . \quad (3)$$

Results were very similar to those obtained with three binding sites (Scheme 2), namely adequate fits of the open and shut time distributions (Fig. 7), similar rate constant values, and a predicted Hill slope of 2.1. The fit is slightly better (because there are more free parameters), but the improvement is not obvious by eye, and the values of the rate constants for the fourth and fifth bindings were not very well defined (Table 4, third column of rate constants). In summary, at least three glycine molecules must bind for efficacious opening of the glycine channel; if a fourth and fifth molecule bind, their ability to open the channel is not greatly different from having only three bound.

Are the sites different before agonist binds?

The rates obtained from fitting Scheme 1 with the hypothesis of saturated gating are very similar to those obtained from the free fits of Scheme 2 (Tables 4 and 5, compare corresponding rates) and thus imply an interaction between binding sites when the channel is still shut. Such interaction is positive for the second binding but negative for the third. It is difficult to explain such a mixed cooperativity in a receptor in which all of the subunits are identical; thus, we considered the possibility that the binding sites are initially different. The idea that the binding sites in a homomeric pentamer are initially different does not seem very plausible, because such structures usually show a high degree of symmetry [however, for biochemical evidence of different subunit

Table 4. Fit of Scheme 1 (five binding sites) to single-channel data

	Unit	Scheme 1, noninteracting binding sites	Coefficient of variation (%)	Scheme 1, free fit	Coefficient of variation (%)	Scheme 1, saturated gating	Coefficient of variation (%)
α_1	s^{-1}	590000	26	201000	34	4000	2
β_1	s^{-1}	110	63	40	86	1300	8
α_2	s^{-1}	6400	2	5000	10	1300	5
β_2	s^{-1}	26	12	1050	30	9300	6
α_3	s^{-1}	1900	4	1800	17	750	6
β_3	s^{-1}	3000	6	6100	21	30200	4
α_4	s^{-1}	960	4	970	4	750	6
β_4	s^{-1}	10200	3	20500	17	30200	4
α_5	s^{-1}	590	3	860	26	750	6
β_5	s^{-1}	21400	3	47300	22	30200	4
k_{-5}	s^{-1}	180	4	4300	70	2800	73
k_{+1}	$M^{-1}s^{-1}$	1.0×10^6	6	7.0×10^6	50	1.2×10^6	53
k_{-4}	s^{-1}	180	4	1200	13	14300	60
k_{+2}	$M^{-1}s^{-1}$	1.0×10^6	6	8.2×10^6	32	150×10^6	93
k_{-3}	s^{-1}	180	4	5910	21	3600	12
k_{+3}	$M^{-1}s^{-1}$	1.0×10^6	6	7.1×10^6	19	2.4×10^6	16
k_{-2}	s^{-1}	180	4	280	9	1200	9
k_{+4}	$M^{-1}s^{-1}$	1.0×10^6	6	0.8×10^6	31	5.6×10^6	6
k_{-1}	s^{-1}	180	4	346	33	400	3
k_{+5}	$M^{-1}s^{-1}$	1.0×10^6	6	0.3×10^6	66	0.1×10^6	12
E_1		2.4×10^{-4}	65	1.2×10^{-5}	56	0.3	8
E_2		4.0×10^{-3}	11	2.4×10^{-1}	31	8	12
E_3		2	7	5	28	42	5
E_4		11	7	22	18	42	5
E_5		37	6	57	8	42	5
K_5	M	180×10^{-6}	3	515×10^{-6}	20	2600×10^{-6}	36
K_4	M	180×10^{-6}	3	310×10^{-6}	28	800×10^{-6}	23
K_3	M	180×10^{-6}	3	80×10^{-6}	6	1600×10^{-6}	10
K_2	M	180×10^{-6}	3	600×10^{-6}	30	200×10^{-6}	5
K_1	M	180×10^{-6}	3	2100×10^{-6}	29	5200×10^{-6}	14
EC_{50}	μM	97		98		97	
Maximum P_{open}		0.97		0.98		0.98	
Hill slope		2.2		3.1		2.1	

Six different sets of experiments done at four different concentrations were fitted with a mechanism with five binding sites and five open states using different constraints. The names of the rate constants are shown in Figure 3 (Scheme 1). Efficacies (E) are defined as the ratios between the corresponding β and α for each gating step, whereas the equilibrium constants for binding (K) are the ratios between k_- and k_+.

The first column shows the mean rates obtained from fits in which the five binding sites were constrained to be identical and noninteracting (and thus all K values are the same). Errors, expressed as coefficient of variation of the mean are in the second column. Rates and errors from the fit to the same model, but with no constraints, are shown in columns 3 and 4, whereas columns 5 and 6 contain the rates and errors from fits in which the last three gating steps were constrained to be identical (saturated gating).

The EC_{50}, maximum P_{open}, and Hill slope calculated from the rate constants are shown on the last three lines, below the corresponding set of rates.

conformations within homomeric nicotinic α7 receptors, see Rakhilin et al. (1999)]. The lack of crystal structures for homooligomeric proteins with no ligand bound means that the evidence on this point is limited. Attempts to fit our data with mechanisms in which the sites were inherently different and noninteracting never led to an adequate fit of the data.

A mechanism with minimal interaction between subunits

In a homomeric receptor, it seems reasonable to assume that all sites are initially equivalent, but that they might no longer be symmetrical once the first agonist molecule has bound. In that case, there would be two distinct doubly liganded states that differ depending on the relative position of the two occupied binding sites. This line of thought led to Scheme 3 (Fig. 8). Two forms of this scheme were fitted, the first one (excluding the grayed states) had three binding sites and the second had five (Scheme 3 with saturated gating).

Attempts to fit Scheme 3 with three binding sites with all parameters free led to good fits of the data, but the values of some of the rate constants were badly defined (Table 6, first column, first set of rate constants). We therefore tried the more interesting idea that there is no interaction at all between the second and third binding. This is achieved by fitting with the following constraints:

$$k_{+2d} = k_{+3d}, \qquad k_{-2d} = k_{-3d}, \qquad k_{-2c} = k_{-3c}. \qquad (4)$$

The fourth constraint, $k_{+2c} = k_{+3c}$, was implied by the requirement of microscopic reversibility for the cycle. The number of free parameters is thus reduced by three, but nonetheless good fits were obtained, as shown in Figure 9. The calculated distributions are qualitatively similar to the ones obtained for fits to Scheme 2, and both the correlations and the P_{open} curve are in excellent agreement with the data. Efficacy increased with the number of bound molecules, and the two doubly liganded open states have different gating constants. More importantly, however, of the two nonequivalent binding steps, one is 10 times faster than the other (Table 6). It is appealing that a good fit can be obtained with the assumption that the second and third bindings to the shut state do not interact; however, it is still necessary to suppose that the first binding can affect other sites while the channel is still shut (see above).

One possible structural interpretation of Scheme 3 is illustrated in Figure 9*c*. According to this interpretation, the first

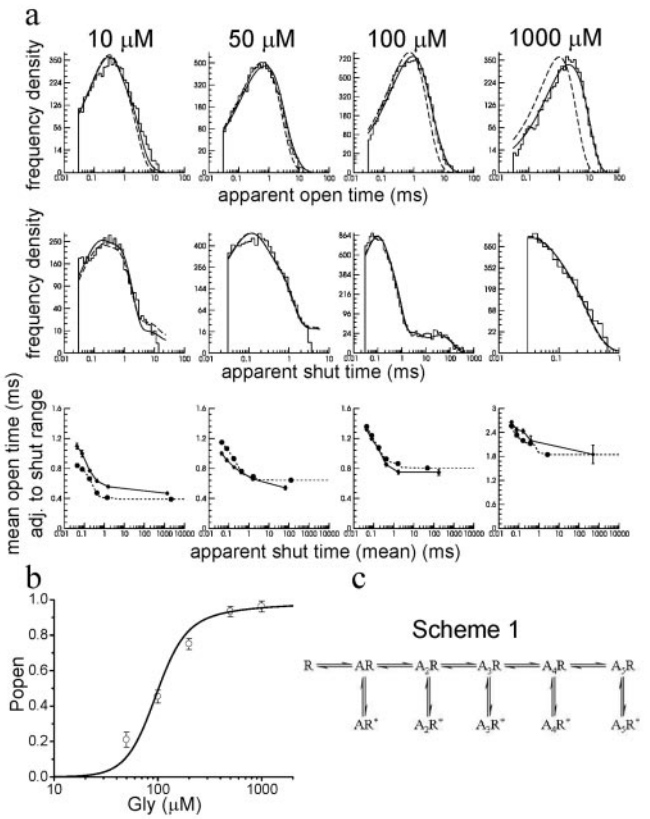

Figure 5. *a*, HJC fitting of Scheme 1 (5 interacting binding sites, *c*) to data from patches at four different glycine concentrations. As in Figure 4, the plots show how well the fitted rate constants with this mechanism predict the experimental observations, whether they are open-time and shut-time distributions (top two rows) or open–shut correlations (third row). Note that the substantial improvement in the description of dwell times and correlations is associated with a marked failure in the description of the slope of the P_{open} dose–response curve (*b*).

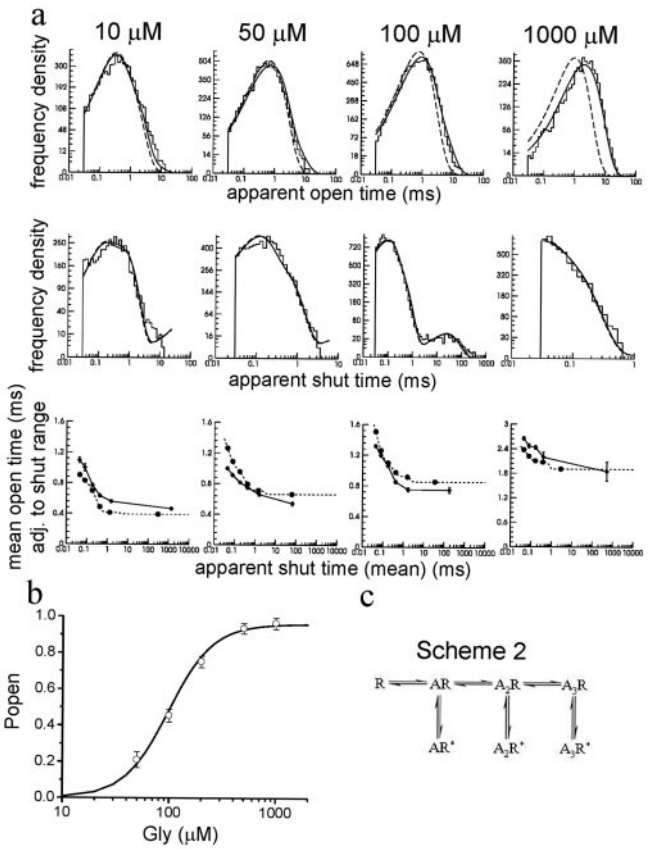

Figure 6. *a*, HJC fitting of Scheme 2 (3 independent binding sites) to data from patches at four different glycine concentrations. As in Figures 4 and 5, the plots show how well the rate constants fitted with this mechanism predict the experimental observations. Note the overall good quality of the predicted distributions or relationships with the experimental data shown in the plots. *b*, P_{open} dose–response curve calculated from the fitted rate constants of Scheme 2 (*c*).

agonist molecule can bind to any of five identical binding sites. However, once the first molecule is bound, the remaining binding sites are no longer equivalent. The binding of the second molecule can occur either on one of the two adjacent binding sites or on one of the other two (nonadjacent) sites. Thus, there are two possible distinct shut configurations with two agonist molecules bound. Additional binding can again occur either between two empty subunits (one available site left) or between one empty and one occupied subunit (with two available sites). Note that of all possible configurations with three bound molecules, we excluded the one with three adjacent agonist molecules bound. This would have given rise to one more fully bound shut state. According to this topological interpretation, the constraints that were used for the fits in Figure 9 should be corrected with the appropriate statistical factors, namely:

$$k_{+2d} = 2k_{+3d} \qquad k_{-2d} = 2k_{-3d} \qquad k_{-2c} = k_{-3c}. \quad (5)$$

As above, the fourth constraint, $k_{+2c} = k_{+3c}$, is a consequence of microscopic reversibility for the cycle. Imposing these constraints has no noticeable effect on the quality of the fits shown in Figure 9 (i.e., Scheme 3) and affects only the estimates of rate constants shown in the third set of rates in Table 6.

The fits of Scheme 3 shown in Figure 9 were for the three-binding site version. Similarly, good fits were also obtained with the five-binding site version of Scheme 3 (i.e., including the states shown in gray in Fig. 8) with the constraints that the gating saturated after the third binding as in Figure 7 (Eq. 3). Adding these

Table 5. Fit of Scheme 2 (three binding sites) to single-channel data

	Unit	Scheme 2, free fit	Coefficient of variation (%)
α_1	s^{-1}	3900	3
β_1	s^{-1}	1300	9
α_2	s^{-1}	1260	6
β_2	s^{-1}	9600	10
α_3	s^{-1}	820	10
β_3	s^{-1}	35300	9
k_{-3}	s^{-1}	2600	20
k_{+3}	$M^{-1}s^{-1}$	7.0×10^6	22
k_{-2}	s^{-1}	1200	13
k_{+2}	$M^{-1}s^{-1}$	11.1×10^6	6
k_{-1}	s^{-1}	420	3
k_{+1}	$M^{-1}s^{-1}$	0.1×10^6	12
E_1		0.4	13
E_2		8	20
E_3		43	5
K_3	M	420×10^{-6}	10
K_2	M	110×10^{-6}	11
K_1	M	3200×10^{-6}	16
EC_{50}	μM	103	
Maximum P_{open}		0.98	
Hill slope		2.1	

Average rates obtained from fitting the data to Scheme 2, with three binding sites and no additional constraints on the rate constants. Note the pattern of increasing and decreasing equilibrium binding constants with an increasing number of bound molecules. The EC_{50}, maximum P_{open}, and Hill slope calculated from the corresponding rate constants are shown on the last three lines.

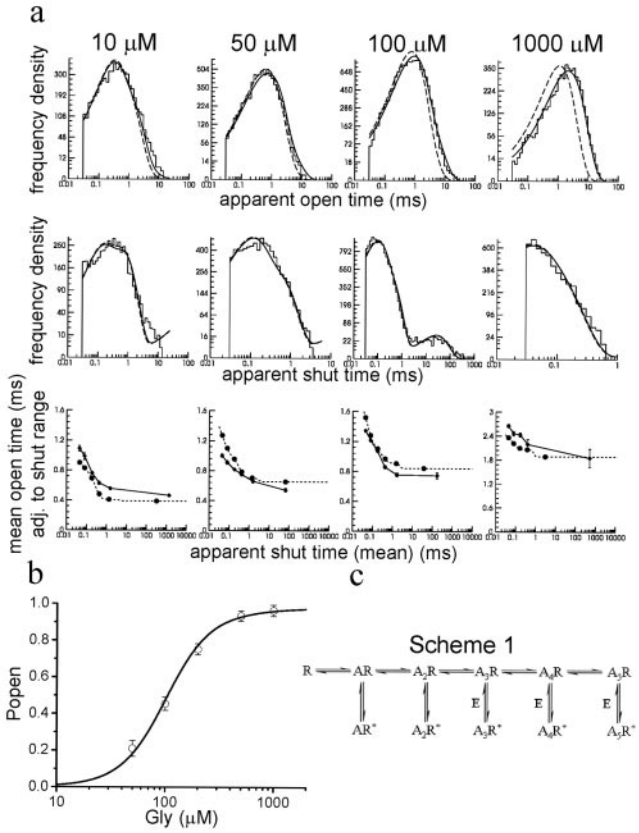

Figure 7. *a*, HJC fitting of Scheme 1 in the hypothesis of saturation of gating after the third agonist molecule is bound (this is indicated in *c* by the same gating constant (*E*) displayed over these gating steps). The agreement of the HJC distributions with the data is excellent. *b*, The P_{open} curve generated by the fitted rates describes the data well.

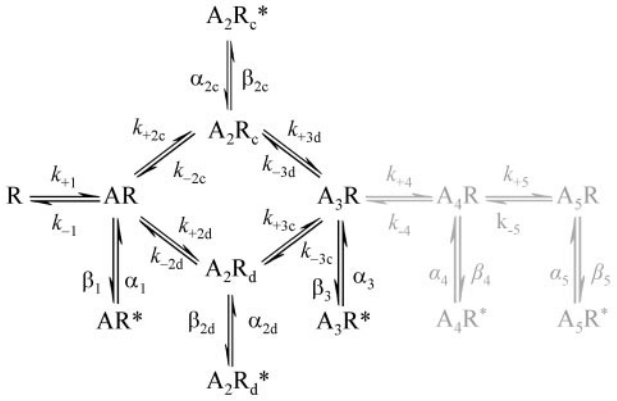

Figure 8. Schematic representation of a mechanism of activation in which there are two distinct diliganded states. This scheme was fitted with and without the fourth and fifth binding, which are shown in gray (see Results).

extra states did not improve the quality of the fits and the estimate of EC_{50} and Hill slope, and we cannot determine whether or not the fourth and fifth bindings occur.

Discussion

In our cell-attached recordings of homomeric α1 glycine single channels, we found that longer lived, more highly liganded open states became more common as glycine concentrations increased over a 100-fold range (Beato et al., 2002). At the higher agonist concentrations, activations became grouped into clusters separated by desensitized intervals (Takahashi and Momiyama, 1991), allowing the construction of a P_{open} concentration–response curve. Plausible receptor activation mechanisms were fitted directly to the sequence of open and shut times, giving rate constants for the binding and gating steps. The success of each model in describing channel behavior was tested by checking how well observed dwell-time distributions and P_{open} curve parameters were matched by those calculated from the fitted rate constant values.

The number of binding sites and the choice of a suitable model

It has often been assumed that more than three glycine molecules must bind to produce efficient channel opening, simply because macroscopic dose–response curves are fairly steep, with reports of Hill slopes up to 4.2 (Bormann et al., 1993). However, Hill slopes are impossible to interpret mechanistically in the absence of a specified model (other than as a minimum for the number of binding sites). Even more importantly, macroscopic dose–response curves are susceptible to distortion by desensitization. Our estimate of the Hill slope which is obtained from the P_{open} curve and is therefore unaffected by desensitization, is lower, approximately 1.8.

Another approach to the determination of the number of binding sites is the analysis of the rising phase of macroscopic current responses to glycine concentration jumps recently reported by Gentet and Clements (2002) for homomeric receptors. This was interpreted to suggest that two agonist molecules must bind (with negative cooperativity) to produce efficient receptor activation. It has also been suggested that full occupancy of the five potential binding sites is not necessary for efficacious gating of $GABA_C$ and 5-HT3 receptors (Amin and Weiss, 1996; Mott et al., 2001).

Our previous work indicated that low-concentration single-channel data were compatible with a model with five binding sites (Beato et al., 2002). Over the wider concentration range, we now found that a free fit with five binding sites (Figs. 3, 5, Scheme 1) could indeed describe the single-channel data well but predicted a Hill slope substantially higher than observed. To get a good fit of the Hill slope with a model with five binding sites, it is necessary to suppose that there is little or no increase in efficacy after three glycine molecules have bound (Fig. 7). Some physical plausibility is lent to this saturation of gating after the third binding by thinking in terms of the breaking of bonds that form the hydrophobic girdle that keeps the channel shut (Colquhoun et al., 2003b; Miyazawa et al., 2003). The third, fourth, and fifth such bonds to be broken must all be adjacent to a bond that has already been broken and might therefore have similar properties. However, we cannot distinguish this case from mechanisms that allow only three molecules to be bound; these also gave a good description of single-channel results, Hill slope, and EC_{50} and have the advantage of being the simplest model that accounts for the data.

A possible way to resolve the uncertainty would be to use fast concentration jumps. After rapid removal of glycine, the decline of response would in principle be more sigmoid if five agonist molecules are bound than with three, although the values of the rate constants found in our fits predict only a small difference. Both schemes predict that the major slowest decay time constant would be between 5 and 8 ms, which is consistent with the results of concentration jumps and with recordings of glycinergic synaptic currents. The 20–80% rise times predicted (by the best fits to Schemes 2 and 3) are approximately 0.2 ms for responses to 1 ms concentration jumps to 3 mM glycine, a value which, again, is in broad agreement with the experimental results of jumps on

Table 6. Fit of Scheme 3 (with three binding sites) to single-channel data

	Unit	Scheme 3, free fit	Coefficient of variation (%)	Scheme 3, no interaction	Coefficient of variation (%)	Scheme 3, no interaction (statistical factors)	Coefficient of variation (%)
α_1	s^{-1}	4300	5	4100	2	4110	3
β_1	s^{-1}	1100	12	1200	7	1200	8
α_{2c}	s^{-1}	1300	7	1300	4	1200	5
β_{2c}	s^{-1}	11200	10	7700	3	7900	4
α_{2d}	s^{-1}	1700	12	1500	11	2200	19
β_{2d}	s^{-1}	4200	12	18300	26	24800	14
α_3	s^{-1}	780	5	790	3	790	4
β_3	s^{-1}	36400	11	32700	4	33900	3
k_{-3d}	s^{-1}	49500	96	6200	10	6400	9
k_{+3d}	$M^{-1}s^{-1}$	61.4×10^6	95	6.8×10^6	10	6.5×10^6	9
k_{-3c}	s^{-1}	6100	24	1600	13	1500	8
k_{+3c}	$M^{-1}s^{-1}$	10.0×10^6	7	16.3×10^6	17	14.1×10^6	12
k_{-2d}	s^{-1}	500	22	6200	10	12700	9
k_{+2d}	$M^{-1}s^{-1}$	3.6×10^6	45	6.8×10^6	10	13.0×10^6	9
k_{-2c}	s^{-1}	2700	13	1600	13	1500	8
k_{+2c}	$M^{-1}s^{-1}$	19.4×10^6	8	16.3×10^6	17	14.1×10^6	12
k_{-1}	s^{-1}	500	4	440	4	430	3
k_{+1}	$M^{-1}s^{-1}$	0.5×10^6	9	0.5×10^6	8	0.5×10^6	8
E_1		0.3	17	0.3	6	0.3	7
E_{2c}		9	15	6	5	7	8
E_{2d}		3	20	12	20	13	19
E_3		47	9	42	5	43	5
K_{3d}	M	710×10^{-6}	11	910×10^{-6}	8	1000×10^{-6}	13
K_{3c}	M	600×10^{-6}	23	100×10^{-6}	5	110×10^{-6}	5
K_{2d}	M	220×10^{-6}	33	910×10^{-6}	8	1000×10^{-6}	13
K_{2c}	M	140×10^{-6}	11	100×10^{-6}	5	110×10^{-6}	5
K_1	M	1000×10^{-6}	12	980×10^{-6}	10	930×10^{-6}	8
EC_{50}	μM	89		96		97	
Maximum P_{open}		0.98		0.98		0.98	
Hill slope		2.0		2.0		2.0	

Rates obtained from fitting of Scheme 3 (Fig. 8) with three different sets of constraints; column 1 shows the rate for unconstrained fits, whereas in column 3, the second and third binding are constrained to be noninteracting. In column 5, the second and third binding are still not interacting, but the rates have been constrained in order to take into account the number of available adjacent and distal binding sites once the first molecule of agonist is bound. The three bottom lines show the EC_{50}, maximum P_{open}, and Hill slope calculated from the corresponding rate constants.

recombinant α1 receptors (0.15–0.2 ms) (Legendre et al., 2002) and recordings of glycinergic synaptic current in rat spinal cord (0.5 ms; note that the composition of these synaptic glycine receptors is not known with certainty) (Jonas et al., 1998).

Cooperativity and interaction between subunits

A very basic but still mostly unanswered question about ion channels concerns whether binding to one site can affect binding to another while the channel is still shut. Such interactions may be more apparent than real. Binding of oxygen to hemoglobin, for example, shows a strong reduction in equilibrium constant for each successive binding if fitted as a simple binding equation (the Adair equation). It was a major insight by Wyman and Allen (1951) to suggest that most, if not all, of this apparent change in affinity was actually the result of a conformation change. This was put in quantitative form in the Monod–Wyman–Changeux mechanism (Monod et al., 1965), in which binding to subunits in one conformation (the shut channel in our case) is the same, regardless of binding to other subunits. However, the ligand bound with higher affinity to another conformation (the open channel) and pushed the conformation equilibrium toward the form with higher affinity, thus giving the appearance of increasing affinity.

Schemes 1 and 2 (with five or three binding sites, respectively) were fitted initially with the constraint that all binding rate constants be the same, thus implying no cooperativity in binding to the shut state, in the spirit of Monod et al. (1965). In all cases, fits failed to describe accurately our experimental single-channel distributions. In muscle nicotinic receptors, affinity decreases (in mouse or *Torpedo* channels) (Jackson, 1988; Sine et al., 1990) or increases slightly (Colquhoun and Sakmann, 1985) from the first to the second agonist binding step; however, these changes cannot be attributed unequivocally to differences in the sites before the agonist binds (heterogeneity), rather than to an interaction between sites (true cooperativity), as pointed out by Colquhoun and Sakmann (1985) and Sine et al. (1990). Almost all fitting to nicotinic receptor data has assumed that binding to one subunit is unaffected by binding to another (Salamone et al., 1999; Hatton et al., 2003). Indeed, it is almost impossible to estimate all of the rate constants (in a model in which the two sites are initially different), unless the assumption that sites do not interact is made (Colquhoun et al., 2003a). Similar assumptions have been made for $GABA_A$ and glycine receptors (Jones and Westbrook, 1995; Legendre, 1998).

Nevertheless, Hatton et al. (2003) found that to fit simultaneously single-channel data for nicotinic receptors at a wide concentration range, it was necessary either to assume some degree of interaction between binding to different sites or to include an extra short-lived (1 ms) shut state, and it was not possible to distinguish between these two possibilities. Far less can it be expected that macroscopic data (e.g., concentration jumps) could resolve the question (Gentet and Clements, 2002; Mozrzymas et al., 2003). However, the evidence for interaction between subunits is rather strong in the present work.

In the rates obtained from the fitting of Scheme 2, the values of the dissociation rate constants for unbinding from the shut channel (after correction with the proper statistical factor) (Table 5)

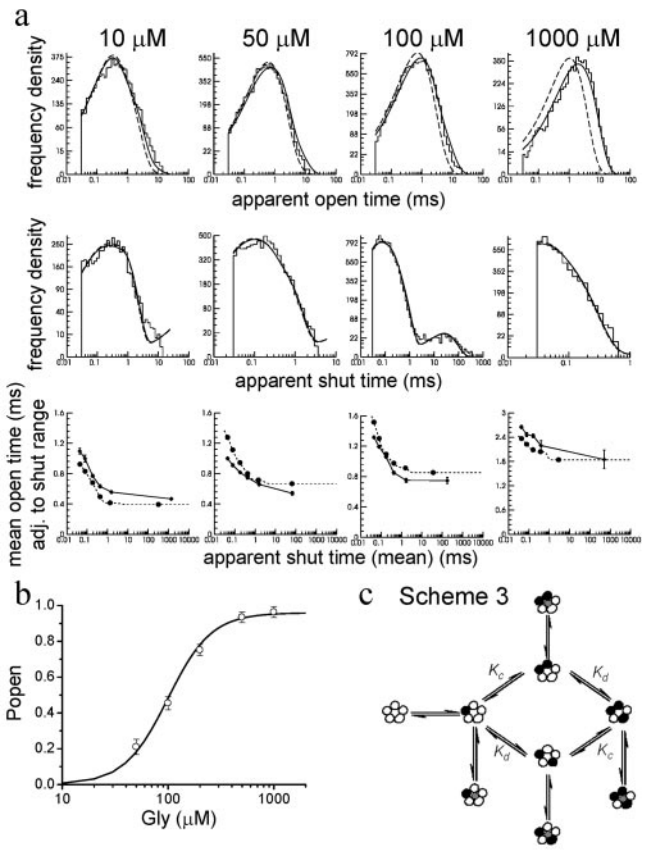

Figure 9. HJC fitting of Scheme 3, which incorporates two distinct independent diliganded shut states (compare Fig. 3), to data from patches at four different glycine concentrations (*a*, *b*). As in Figure 4, the plots show how well the fitted rate constants with this mechanism predict the experimental observations. Note the overall good agreement of the description of the different categories of data; this is similar to the quality of the predictions of Scheme 2 (Fig. 6). *c*, Interpreting the relationship between binding kinetics and state of ligation for a homomeric receptor. The mechanism shown here is the same as the scheme in Figure 8 but adds a realistic interpretation of the binding cooperativity, in view of the possible arrangements of binding sites. Each of the five circles represents a binding site, which can be either empty (open circle) or occupied by agonist (filled circle); open states of the channel are indicated by a shaded pore in the middle of the pentamer. The constraints used in the fits are indicated by the binding constants (either K_c or K_d) displayed over the second and third binding steps.

increases as the number of bound molecules increases for one to three. This implies negatively cooperative interactions between binding sites in the shut conformation, in the sense that dissociation is faster when other sites are occupied. In contrast, the association rate constants (all quite slow compared with nicotinic receptors) seem to show positively cooperative interactions, being slow (0.1 $\mu M^{-1}s^{-1}$) for the first binding but increasing to 7–10 $\mu M^{-1}s^{-1}$ for subsequent bindings. It is quite hard to imagine a physically realistic mechanism for such an interaction. One possibility is that the interaction is mediated by a substantial change in conformation produced by binding while the channel is still shut. If that was so, this conformation change should really be incorporated into the mechanism, but attempts to use a stepwise gating model have been few for receptors in this superfamily (Colquhoun and Ogden, 1988; Auerbach, 1993), and it seems unlikely that such a kinetic step could be resolved.

Another possibility is an electrostatic effect between bound agonist molecules. These interactions operate at short range in aqueous medium (3 Å for the negative cooperativity in the protonation of the amino acid glycine) (Wyman and Gill, 1990). However, this range could be greater in the interior of a protein, which has a lower dielectric constant than an aqueous ionic solution (Dwyer et al., 2000), and it might be comparable with the distance between adjacent binding sites (approximately 20 Å, judging by the snail ACh-binding protein structure) (Brejc et al., 2001).

An electrostatic interaction would explain the asymmetry of the second binding in Scheme 3, in terms of binding to a subunit that is adjacent or distal to the site where the first binding occurred. It is also possible that such topological interaction results from a conformational change while the channel is still shut. However, the present knowledge of the structure of open and shut states and of the path between them is insufficient to make any predictions of the nature of interactions between subunits, and *a fortiori*, of how binding rate constants would be expected to vary with degree of ligation.

Conclusions

The efficacy of gating increases with the level of ligation, as in muscle nicotinic (Colquhoun and Sakmann, 1985) and $GABA_A$ receptors (Jones and Westbrook, 1995). Whether or not we include a fourth and fifth binding, it reaches a maximum of approximately 40, a value which predicts a maximum P_{open} of 0.98, which is very close to the observed value.

We have no compelling reason from our steady-state measurements to invoke a fourth and fifth binding (Fig. 8, gray states), other than to point out that if they did not occur, it would imply a very strong negative interaction. This uncertainty may be resolved by concentration jump experiments. We cannot explain all of our results without invoking some interaction between binding sites while the channel is still in the shut conformation. The topological binding interpretation has the advantage of giving a simple physical interpretation of the observed variation in the binding equilibrium constants. This still implies some interaction between subunits in the shut conformation after binding of the first (but not subsequent) glycine molecules but takes into account the physical nature of the binding sites of the receptor.

References

Amin J, Weiss DS (1996) Insights into the activation mechanism of ρ1 GABA receptors obtained by coexpression of wild type and activation impaired subunits. Proc R Soc Lond B Biol Sci 263:273–282.

Auerbach A (1993) A statistical analysis of acetylcholine receptor activation in *Xenopus* myocytes: stepwise *versus* concerted models of gating. J Physiol (Lond) 461:339–378.

Beato M, Groot-Kormelink PJ, Colquhoun D, Sivilotti LG (2002) Openings of the rat recombinant α1 homomeric glycine receptor as a function of the number of agonist molecules bound. J Gen Physiol 119:443–466.

Bormann J, Rundström N, Betz H, Langosch D (1993) Residues within transmembrane segment M2 determine chloride conductance of glycine receptor homo- and hetero-oligomers. EMBO J 12:3729–3737.

Brejc K, van Dijk WJ, Klaassen RV, Schuurmans M, van der Oost J, Smit AB, Sixma TK (2001) Crystal structure of an ACh-binding protein reveals the ligand-binding domain of nicotinic receptors. Nature 411:269–276.

Colquhoun D (1998) Binding, gating, affinity and efficacy: the interpretation of structure-activity relationships for agonists and of the effects of mutating receptors. Br J Pharmacol 125:923–947.

Colquhoun D, Hawkes AG (1990) Stochastic properties of ion channel openings and bursts in a membrane patch that contains two channels: evidence concerning the number of channels present when a record containing only single openings is observed. Proc R Soc Lond B Biol Sci 240:453–477.

Colquhoun D, Hawkes AG (1995) The principles of the stochastic interpretation of ion-channel mechanisms. In: Single-channel recording (Sakmann B, Neher E, eds), pp 397–482. New York: Plenum.

Colquhoun D, Ogden DC (1988) Activation of ion channels in the frog

end-plate by high concentrations of acetylcholine. J Physiol (Lond) 395:131–159.
Colquhoun D, Sakmann B (1985) Fast events in single-channel currents activated by acetylcholine and its analogues at the frog muscle end-plate. J Physiol (Lond) 369:501–557.
Colquhoun D, Sigworth FJ (1995) Fitting and statistical analysis of single-channel records-channel mechanisms. In: Single-channel recording (Sakmann B, Neher E, eds), pp 483–587. New York: Plenum.
Colquhoun D, Hawkes AG, Srodzinski K (1996) Joint distributions of apparent open and shut times of single-ion channels and maximum likelihood fitting of mechanisms. Philos Trans R Soc Lond A 354:2555–2590.
Colquhoun D, Hatton CJ, Hawkes AG (2003a) The quality of maximum likelihood estimates of ion channel rate constants. J Physiol (Lond) 547:699–728.
Colquhoun D, Unwin N, Shelley C, Hatton CJ, Sivilotti L (2003b) Nicotinic acetylcholine receptors. In: Burger's medicinal chemistry and drug discovery: fundamentals of medicinal chemistry (Abraham D, ed), pp 357–405. New York: Wiley.
Dwyer JJ, Gittis AG, Karp DA, Lattman EE, Spencer DS, Stites WE, Garcia-Moreno EB (2000) High apparent dielectric constants in the interior of a protein reflect water penetration. Biophys J 79:1610–1620.
Edmonds B, Gibb AJ, Colquhoun D (1995) Mechanisms of activation of muscle nicotinic acetylcholine receptors, and the time course of endplate currents. Annu Rev Physiol 57:469–493.
Gentet LJ, Clements JD (2002) Binding site stoichiometry and the effects of phosphorylation on human α1 homomeric glycine receptors. J Physiol (Lond) 544:97–106.
Groot-Kormelink PJ, Beato M, Finotti C, Harvey RJ, Sivilotti LG (2002) Achieving optimal expression for single channel recording: a plasmid ratio approach to the expression of α1 glycine receptors in HEK293 cells. J Neurosci Methods 113:207–214.
Grosman C, Auerbach A (2000) Kinetic, mechanistic, and structural aspects of unliganded gating of acetylcholine receptor channels: a single-channel study of second transmembrane segment 12′ mutants. J Gen Physiol 115:621–635.
Hatton CJ, Shelley C, Brydson M, Beeson D, Colquhoun D (2003) Properties of the human muscle nicotinic receptor, and of the slow-channel myasthenic syndrome mutant epsilonL221F, inferred from maximum likelihood fits. J Physiol (Lond) 547:729–760.
Hawkes AG, Jalali A, Colquhoun D (1990) The distributions of the apparent open times and shut times in a single channel record when brief events can not be detected. Philos Trans R Soc Lond A 332:511–538.
Hawkes AG, Jalali A, Colquhoun D (1992) Asymptotic distributions of apparent open times and shut times in a single channel record allowing for the omission of brief events. Philos Trans R Soc Lond B Biol Sci 337:383–404.
Jackson MB (1988) Dependence of acetylcholine receptor channel kinetics on agonist concentration in cultured mouse muscle fibres. J Physiol (Lond) 397:555–583.
Jonas P, Bischofberger J, Sandkuhler J (1998) Co-release of two fast neurotransmitters at a central synapse. Science 281:419–424.
Jones MV, Westbrook GL (1995) Desensitized states prolong $GABA_A$ channel responses to brief agonist pulses. Neuron 15:181–191.
Legendre P (1998) A reluctant gating mode of glycine receptor channels determines the time course of inhibitory miniature synaptic events in zebrafish hindbrain neurons. J Neurosci 18:2856–2870.
Legendre P (2001) The glycinergic inhibitory synapse. Cell Mol Life Sci 58:560–593.
Legendre P, Muller E, Badiu CI, Meier J, Vannier C, Triller A (2002) Desensitization of homomeric α1 glycine receptor increases with receptor density. Mol Pharmacol 62:817–827.
Lewis TM, Sivilotti L, Colquhoun D, Schoepfer R, Rees M (1998) Properties of human glycine receptors containing the hyperekplexia mutation α1 (K276E), expressed in *Xenopus* oocytes. J Physiol (Lond) 507:25–40.
Lewis TM, Schofield PR, McClellan AM (2003) Kinetic determinants of agonist action at the recombinant human glycine receptor. J Physiol (Lond) 549:361–374.
Miyazawa A, Fujiyoshi Y, Unwin N (2003) Structure and gating mechanism of the acetylcholine receptor pore. Nature 423:949–955.
Monod J, Wyman J, Changeux J-P (1965) On the nature of allosteric transitions: a plausible model. J Mol Biol 12:88–118.
Mott DD, Erreger K, Banke TG, Traynelis SF (2001) Open probability of homomeric murine $5\text{-}HT_{3A}$ serotonin receptors depends on subunit occupancy. J Physiol (Lond) 535:427–443.
Mozrzymas JW, Barberis A, Mercik K, Zarnowska ED (2003) Binding sites, singly bound states, and conformation coupling shape GABA-evoked currents. J Neurophysiol 89:871–883.
Qin F, Auerbach A, Sachs F (1996) Estimating single-channel kinetic parameters from idealized patch-clamp data containing missed events. Biophys J 70:264–280.
Rajendra S, Schofield PR (1995) Molecular mechanisms of inherited startle syndromes. Trends Neurosci 18:80–82.
Rajendra S, Lynch JW, Pierce KD, French CR, Barry PH, Schofield PR (1994) Startle disease mutations reduce the agonist sensitivity of the human inhibitory glycine receptor. J Biol Chem 269:18739–18742.
Rakhilin S, Drisdel RC, Sagher D, McGehee DS, Vallejo Y, Green WN (1999) α-bungarotoxin receptors contain α7 subunits in two different disulfide-bonded conformations. J Cell Biol 146:203–217.
Salamone FN, Zhou M, Auerbach A (1999) A re-examination of adult mouse nicotinic acetylcholine receptor channel activation kinetics. J Physiol (Lond) 516:315–330.
Sine SM, Steinbach JH (1987) Activation of acetylcholine receptors on clonal mammalian BC3H-1 cells by high concentrations of agonist. J Physiol (Lond) 385:325–359.
Sine SM, Claudio T, Sigworth FJ (1990) Activation of *Torpedo* acetylcholine receptors expressed in mouse fibroblasts. Single channel current kinetics reveal distinct agonist binding affinities. J Gen Physiol 96:395–437.
Takahashi T, Momiyama A (1991) Single-channel currents underlying glycinergic inhibitory postsynaptic responses in spinal neurons. Neuron 7:965–969.
Turecek R, Trussell LO (2002) Reciprocal developmental regulation of presynaptic ionotropic receptors. Proc Natl Acad Sci USA 99:13884–13889.
Twyman RE, Macdonald RL (1991) Kinetic properties of the glycine receptor main- and sub-conductance states of mouse spinal cord neurones in culture. J Physiol (Lond) 435:303–331.
Wyman J, Allen DW (1951) The problem of the heme interactions in hemoglobin and the basis of the Bohr effect. J Polymer Science VII:499–518.
Wyman J, Gill SJ (1990) Binding and linkage. In: Functional chemistry of biological macromolecules, p 59. Mill Valley, CA: University Science Books.